



CHORUS

This is the accepted manuscript made available via CHORUS. The article has been published as:

Defect control in the Heisenberg-Kitaev candidate material
math

NaRuO_2

Brenden R. Ortiz, Paul M. Sarte, Alon H. Avidor, and Stephen D. Wilson

Phys. Rev. Materials **6**, 104413 — Published 26 October 2022

DOI: [10.1103/PhysRevMaterials.6.104413](https://doi.org/10.1103/PhysRevMaterials.6.104413)

Defect control in the Heisenberg-Kitaev candidate material NaRuO₂

Brenden R. Ortiz^{†,1,*} Paul M. Sarte^{†,1} Alon H. Avidor¹ and Stephen D. Wilson^{1,‡}

¹*Materials Department, University of California Santa Barbara, Santa Barbara, CA 93106, United States*

(Dated: October 10, 2022)

The combination of geometric frustration, extended hopping, spin-orbit coupling, and a disordered magnetic ground state make NaRuO₂ an attractive Heisenberg-Kitaev candidate material. Historically, NaRuO₂ has been a challenging material to produce, even in polycrystalline form. Here we present synthetic efforts that identify a propensity for Na_{Ru} defects to form in NaRuO₂, revealing a full solid-solution between NaRuO₂ and disordered Na₂RuO₃. We report the synthesis of alloys along the Na_{3+x}Ru_{3-x}O₆ solid solution and characterize changes in the bulk magnetization and electron transport as a function of Na-loading. Our results highlight the importance of stoichiometry control in NaRuO₂ when investigating and interpreting this material’s physical properties.

I. INTRODUCTION

Unambiguous experimental realization of a quantum spin liquid (QSL) state remains an enduring challenge [1–3]. Characterized by a ground state featuring highly entangled spins exhibiting no long-range magnetic order, QSL states are born out of an intricate and often subtle interplay of comparable, often competing, energy scales and are thought to be quenched by relatively small perturbations. Thus, understanding and controlling crystalline disorder, structural distortions, chemical impurities, and intrinsic defects are critical challenges when developing QSL phenomenology in real materials.

NaRuO₂ is a newly proposed, candidate QSL host that straddles a unique energy landscape – one where Heisenberg-Kitaev interactions as well as extended exchange foster a native, quantum disordered ground state [4]. NaRuO₂ is a member of the layered family of ABO₂ delafossite-like oxides, a larger family of *R* $\bar{3}m$ quasi-two-dimensional materials that support ideal antiferromagnetic triangular lattices on the *B*-site sublattice. Specifically, NaRuO₂ (Figure 1) features a triangular lattice of Ru³⁺ ions separated by planes of Na⁺. The edge-sharing RuO₆ octahedra place the Ru³⁺ (4d⁵) ions in a lightly trigonally distorted cubic crystal field. With appreciable spin-orbit coupling λ and Coulomb repulsion U , the system is capable of supporting a half-filled $J_{\text{eff}} = 1/2$ orbital. The result is a weak $J_{\text{eff}} = 1/2$ Mott state with a disordered magnetic ground state and energetic antiferromagnetic interactions [4].

Despite lacking native chemical disorder such as that present in triangular lattice compounds like YbMgGaO₄ [5, 6], off-stoichiometry and the resulting defects are a persistent concern among the alkali metal delafossite variants [7, 8]. The typical culprit tends to be alkali-metal vacancies, whose presence is traditionally countered by the introduction of an excess of alkali precursors during growth. However, the historical precedent for alkali-

vacancies as the dominant defect often neglects complex structure-defect-property relationships that can dominate in real systems – NaRuO₂ is one such example.

In this work, we examine the defect chemistry of the Heisenberg-Kitaev candidate material NaRuO₂, mapping the Na–Ru–O phase diagram in the vicinity of NaRuO₂ to understand the extent and type of off-stoichiometry supported by the compound. We demonstrate the formation of a single solid-solution Na_{3+x}Ru_{3-x}O₆ between the triangular lattice compound NaRuO₂ and the disordered honeycomb lattice compound Na₂RuO₃ [9], highlighting the tendency for NaRuO₂ to form Na-rich Na_{Ru} defects. A combination of bulk magnetization and electron transport measurements highlight strong property changes as a function of Na-loading, highlighting the importance – and more importantly – the ability to control stoichiometry in NaRuO₂.

II. EXPERIMENTAL METHODS

A. Synthesis

Polycrystalline members of the Na_{3+x}Ru_{3-x}O₆ solid solution were synthesized using the same mechanochemical methods detailed in our recent work [4]. Na₂O₂ beads (Sigma, 97%), RuO₂ powder (Alfa, 99.95%), and Na metal (Alfa 99.8%) were combined in a pre-seasoned tungsten carbide ball mill vial and sealed under Ar. Due to the volatility of Na and potential oxygen off-stoichiometry in RuO_{2-x}, adjustments are required to the nominal Na:Ru:O ratios. Specifically, both the compositions for Na₂RuO₃ and NaRuO₂ were empirically tuned to yield phase-pure compositions at Na_{1.07}(RuO₂)_{1.13}(Na₂O₂)_{0.70} (Na_{2.0}Ru_{0.9}O_{3.0}) and Na_{1.07}(RuO₂)_{1.37}(Na₂O₂)_{0.37} (Na_{1.0}Ru_{0.8}O_{2.0}) respectively. Using a combination of excess Na metal, Na₂O₂ and RuO₂, we iteratively narrowed down the single-phase region of the NaRuO₂–Na₂RuO₃ alloy, adjusting the compositional vectors until secondary phases were eliminated. All alloys were generated through a subsequent linear interpolation of the *tuned* compositions of Na₂RuO₃ and NaRuO₂. Empirical tuning and interpo-

* ortiz.brenden@gmail.com; These authors contributed equally

† pmsarte@gmail.com; These authors contributed equally

‡ stephendwilson@ucsb.edu

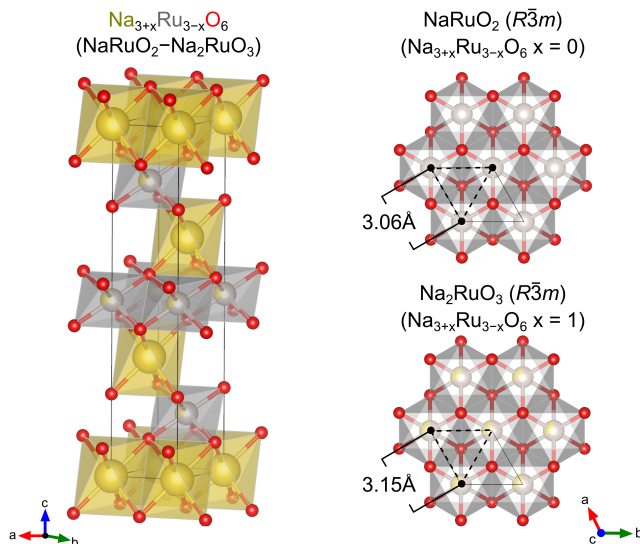


FIG. 1. Delafossite ($R\bar{3}m$) crystal structure assumed by the $\text{Na}_{3+x}\text{Ru}_{3-x}\text{O}_6$ solid solution between the ternary end members NaRuO_2 ($x=0$) and disordered Na_2RuO_3 ($x=1$). $\text{Na}_{3+x}\text{Ru}_{3-x}\text{O}_6$ forms a triangular sublattice comprised of edge-sharing Ru^{3+} ($4d^5$) octahedra. Na-rich conditions overwhelmingly favor formation of Na_{Ru} anti-site defects, diluting the Ru^{3+} sublattice with nonmagnetic Na^+ .

lation is essential, as the compensating ratio of Na:Ru:O that yields phase pure NaRuO_2 is not the same as the compensation required for Na_2RuO_3 .

The resulting mixture was milled for 60 min in a Spex 8000D Mixer/Mill using four 7.9 mm tungsten carbide balls. The reaction generates a substantial amount of heat, and care must be taken with large sample volumes. The resulting precursor is confirmed amorphous by powder x-ray diffraction. The milled powder was then lightly ground in an agate mortar under Ar to disperse any agglomerates, sieved through a 100 micron sieve, and loaded into 2 mL alumina cylindrical crucibles (CoorsTek). In addition, a small portion of the milled powder was cold-pressed into 5 mm diameter pellets and buried within the powder bed. The crucibles were subsequently sealed under 1 atm of Ar in fused silica ampoules and placed within a 900°C preheated furnace. Samples were annealed for 30 min and then immediately air-quenched before extracting powders under Ar. The final powders and sintered pellets are largely phase pure with trace amounts of Ru metal (<2 %). Powders are black and moisture sensitive, with sensitivity increasing dramatically with additional Na content.

B. Structural Characterization

Phase purity was initially examined with powder x-ray diffraction (XRD) measurements at room temperature on a Panalytical Empyrean diffractometer ($\text{Cu K}_{\alpha 1,2}$) in Bragg-Brentano (θ - θ) geometry. $\text{Na}_{3+x}\text{Ru}_{3-x}\text{O}_6$ pow-

ders were placed on a Si zero-diffraction plate under argon and capped with a 12 mm \times 12 mm piece Kapton film to shield against atmospheric moisture. Pawley and Rietveld refinements were performed using TOPAS Academic v6 [10]. Structural models and visualization utilized the VESTA software package [11].

C. Magnetization and Electron Transport Measurements

Temperature dependent dc-magnetization data under zero-field-cooled (ZFC) and field-cooled (FC) conditions were collected on a 7 T Quantum Design Magnetic Property Measurement System (MPMS3) SQUID magnetometer. Samples were sealed in polypropylene holders under argon to minimize absorption of atmospheric moisture. Data was collected continuously in sweep mode with a ramp rate of 2 K/min in the presence of an external DC field of 1000 Oe. Isothermal dc-magnetization measurements at 2 K were collected continuously in sweep mode with a ramp rate of 100 Oe/sec.

Resistivity measurements were performed on sintered pellets of $\text{Na}_{3+x}\text{Ru}_{3-x}\text{O}_6$ that were sectioned into rectangular bars with approximate dimensions of 1 \times 2 \times 0.5 mm. Electrical contacts were made in a standard four-point geometry with contacts being made with a combination of gold wire and silver paint. Thermal contact and electrical isolation was ensured using layers of GE varnish and cigarette paper. The temperature dependence of the electrical resistivity was measured with the Electrical Transport Option (ETO) in a 9 T Quantum Design Dynacool Physical Property Measurement System (PPMS) using a drive current of 10 μA and drive frequency of 100 Hz. Data was collected continuously in sweep mode with a ramp rate of 2 K/min.

III. RESULTS & DISCUSSION

A. Synthesis & Structure

Motivated by the combination of strong spin-orbit coupling, the expanded nature of the Ru d -orbitals, and remnant Coulomb interaction effects, ruthenates have continued to garner substantial attention. Owing to the many stable oxidation states of Ru, the Na-Ru-O phase diagram is remarkably complex. Within a relatively narrow set of chemical potentials there are at least 7 reported Na-Ru-O ternary compounds: NaRuO_2 [12], NaRu_2O_4 [13], Na_2RuO_3 [9], Na_3RuO_4 [14], Na_2RuO_4 [9], $\text{Na}_{27}\text{Ru}_{14}\text{O}_{48}$ [15], and $\text{Na}_{3-x}\text{Ru}_4\text{O}_9$ [16].

NaRuO_2 is of particular interest due to the triangular sublattice of Ru^{3+} and the potential applications as a QSL candidate material [4]. Remarkably, a survey of adjacent phases to NaRuO_2 reveals the “disordered” ($R\bar{3}m$) polymorph of Na_2RuO_3 is structurally identical to NaRuO_2 , except for the random dilution of the Ru^{3+}

triangular sublattice with nonmagnetic Na_{Ru} defects. It is important to note that while Na_2RuO_3 can also crystallize in a ordered $C2/c$ monoclinic structure, it is not clear which phase is the thermodynamic ground state.

Such a relationship and the resulting potential for off-stoichiometry in NaRuO_2 is supported by a comparison to the available crystallographic data. The original synthesis procedure reported for NaRuO_2 involves a three step decomposition process where: 1) Na_2RuO_4 was synthesized from a stoichiometric mixture of Na_2O_2 and RuO_2 , 2) stoichiometric amounts of Na_2RuO_4 and Ru metal were mixed, dried, and sealed inside gold tubing, and finally 3) the mixture was heated at 1173 K for 12 h and then 1273 K for 120 h [13]. This processing route produces material with lattice parameters $[a, c] : [3.02 \text{ \AA}, 16.49 \text{ \AA}]$. We have developed a new, rapid, mechanochemical route for the synthesis of NaRuO_2 [4], which is the method utilized in the present study. This processing route renders NaRuO_2 with lattice parameters $[3.06 \text{ \AA}, 16.18 \text{ \AA}]$.

The difference observed in the c -axis lattice parameters reported in this work [4] and prior work by Shikano et al. [12] is substantial and noteworthy. One potential origin of this discrepancy is the impact of Na off-stoichiometry, which would naturally impact the interlayer spacing. Looking to the analogous titanate structure ($\text{Na}_{1-x}\text{TiO}_2$), detailed structural studies have identified a contraction along c and an expansion in a as Na-vacancies were eliminated and the composition approached nominal NaTiO_2 [8]. We suggest that the smaller c -axis lattice parameter of NaRuO_2 synthesized via the mechanochemical route presented herein are closer to the ideal 1:1:2 stoichiometry. This is further supported by our previous neutron powder diffraction refinement [4], which indicates that the *tuned* NaRuO_2 composition is stoichiometric within the resolution of our measurement. The discrepancy between the prior report and our results suggests that off-stoichiometry and defect control are important factors in NaRuO_2 .

Drawing inspiration from the thermoelectric community and the concept of “phase boundary mapping” [17–20], we sought to map the phase space surrounding NaRuO_2 . Wide swaths of the space immediately surrounding NaRuO_2 are dominated by 2-phase equilibria, which is unexpected if NaRuO_2 is a prototypical line compound. This is instead consistent with the formation of a large single-phase region or an extended alloy. Furthermore, NaRuO_2 shows an unusual proclivity to incorporate excess Na into the structure. Considering the structural similarity of disordered Na_2RuO_3 , we suspected that a solid solution between NaRuO_2 and Na_2RuO_3 could exist. In support of this conjecture, synthesizing Na_2RuO_3 using the same synthetic conditions as NaRuO_2 results in the formation of disordered $R\bar{3}m$ Na_2RuO_3 . This disordered Na_2RuO_3 polymorph persists after extended annealing and appears to be the stable structure under our processing conditions.

To verify the solid-solution hypothesis, a series of sam-

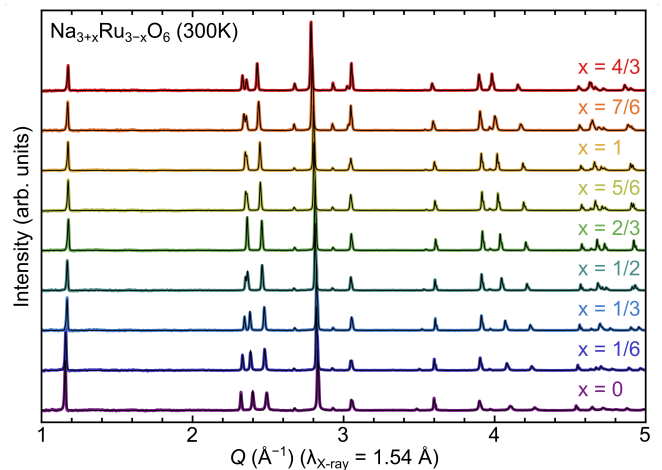


FIG. 2. X-ray patterns of $\text{Na}_{3+x}\text{Ru}_{3-x}\text{O}_6$ alloy series demonstrate Successful alloying of NaRuO_2 ($x=0$) and Na_2RuO_3 ($x=1$) through continuous shifts in the peak positions and intensities. Black traces indicate resulting Pawley refinements in the $R\bar{3}m$ structure. All samples up to $x=1$ are predominantly phase-pure $\text{Na}_{3+x}\text{Ru}_{3-x}\text{O}_6$ with trace Ru metal. Samples extending beyond nominal Na_2RuO_3 ($x=1$) exhibit increased Ru formation, suggesting a geometrical shift in the single-phase boundary.

ples ranging from NaRuO_2 – Na_2RuO_3 were synthesized. For the sake of convenience, we will refer to the series using the renormalized stoichiometry $\text{Na}_{3+x}\text{Ru}_{3-x}\text{O}_6$ where the end members of $x=0$ and $x=1$ correspond to nominal NaRuO_2 and Na_2RuO_3 , respectively. As illustrated in Fig. 2, x-ray diffraction data confirm that the series of alloys constructed along the NaRuO_2 – Na_2RuO_3 pseudobinary phase diagram are predominantly single phase, with a only a small secondary fraction of Ru metal. In the spirit of phase-boundary mapping [17–20], this impurity was intentionally introduced to pin the samples to the Ru-rich edge of the single-phase region. Significant changes in peak positions and the corresponding lattice parameters (Fig. 3) are clearly observed in the x-ray scattering measurements.

A summary of the changes in the crystallographic parameters accompanying the transition from NaRuO_2 to Na_2RuO_3 is presented in Fig. 3. The cell volume increases both monotonically and linearly from NaRuO_2 ($x=0$) to Na_2RuO_3 ($x=1$), consistent with Vegard’s Law. This serves as confirmation of a solid solution, and further highlights the propensity for the formation of Na_{Ru} antisite defects in NaRuO_2 . Unexpectedly, the off-stoichiometry of disordered Na_2RuO_3 is similarly complex and has the ability to absorb excess Na up to $x=4/3$. Past this point, samples become multiphase and exhibit a mixture of Na-rich $\text{Na}_{3+x}\text{Ru}_{3-x}\text{O}_6$ and Na_3RuO_4 . It is interesting to note that the symmetry of Na_3RuO_4 (space group $C2/m$) is a subgroup for $R\bar{3}m$ and is structurally similar to NaRuO_2 and Na_2RuO_3 (e.g. 6-coordinate Na/Ru, approximate planes of metal cations).

The volumetric expansion of the lattice observed in

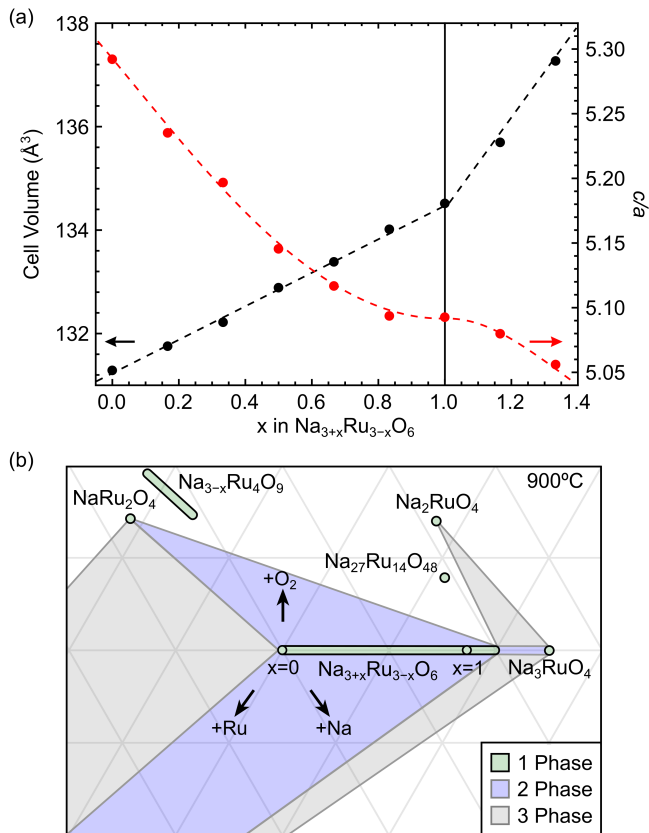


FIG. 3. (a) Compositional dependence of the unit cell volume (black) and the c/a ratio (red) for the $\text{Na}_{3+x}\text{Ru}_{3-x}\text{O}_6$ solid solution extracted from Pawley refinements of room temperature pXRD data. (b) Tentative processing ternary phase diagram schematic at 900°C isotherm for Na–Ru–O space surrounding the $\text{Na}_{3+x}\text{Ru}_{3-x}\text{O}_6$ solid solution.

Fig. 3 with additional Na-loading can be rationalized through simple ionic radii arguments. In a 6-coordinate environment, the Shannon radius of Ru^{3+} is 0.68 \AA and Ru^{4+} is 0.62 \AA . While excess Na is expected to convert Ru^{3+} to Ru^{4+} , the effect of substituting the much larger Na^+ (1.02 \AA) on Ru^{3+} dominates. Thus, a general expansion of the lattice is expected as Na_{Ru} defects accumulate.

The $\text{Na}_{3+x}\text{Ru}_{3-x}\text{O}_6$ solid solution poses a synthetic challenge, particularly when the stoichiometry of polycrystalline NaRuO_2 needs to be tightly controlled. As illustrated in Fig. 3(b), the $\text{Na}_{3+x}\text{Ru}_{3-x}\text{O}_6$ solid solution creates several large 2-phase (blue) regions where $\text{Na}_{3+x}\text{Ru}_{3-x}\text{O}_6$ is at equilibrium with NaRu_2O_4 under O-rich conditions, Ru metal under O-poor conditions, and Na_3RuO_4 under Na-rich conditions. Three unique three-phase (gray) equilibria were identified between $\text{Na}_{3+x}\text{Ru}_{3-x}\text{O}_6$ – NaRu_2O_4 –Ru, $\text{Na}_{3+x}\text{Ru}_{3-x}\text{O}_6$ – Na_2RuO_4 – Na_3RuO_4 , and $\text{Na}_{3+x}\text{Ru}_{3-x}\text{O}_6$ – Na_3RuO_4 –Ru. In our experience, the NaRuO_2 – Na_2RuO_3 alloy does not readily support off-stoichiometry in the Ru-rich direction beyond NaRuO_2 . Employing the principles of

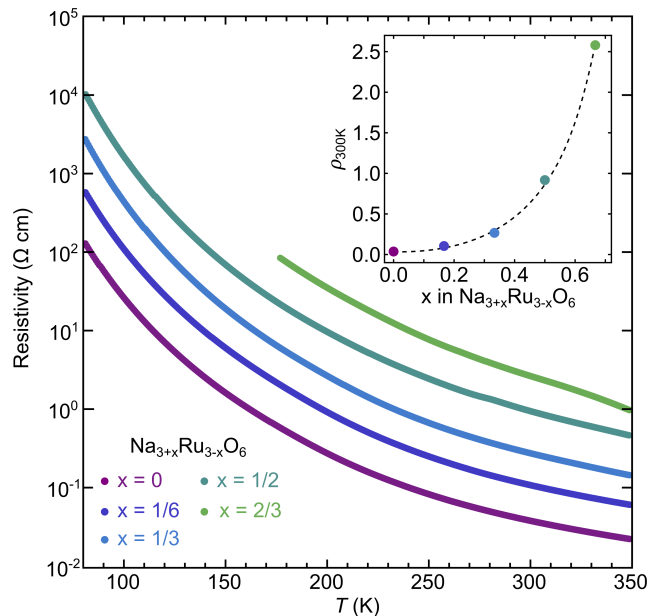


FIG. 4. Temperature dependence of electronic resistivity of $\text{Na}_{3+x}\text{Ru}_{3-x}\text{O}_6$ alloys up to $x = 2/3$ is consistent with a lightly doped insulator, with (inset) resistivity increasing exponentially with Na incorporation.

phase boundary mapping, we would aim to synthesize NaRuO_2 under conditions that place it in equilibrium with NaRu_2O_4 and Ru metal. A convenient metric would be to minimize the cell volume of NaRuO_2 .

Attempts to make samples in the O-rich region above nominal Na_2RuO_3 indicate the presence of *at least one* unknown Na–Ru–O ternary, complicating the mapping process. Although we would naively suspect samples to contain $\text{Na}_{27}\text{Ru}_{14}\text{O}_{48}$ [15], this phase could not be reproduced using the processing techniques described here. Considering the potential complexity in this region of the diagram, we refrain from postulating on the phase equilibria in this region. This is complicated by the existence of the $\text{Na}_{3-x}\text{Ru}_4\text{O}_9$ solid-solution, creating large swaths of 2-phase regions. Future work will be required to fully understand the O-rich side of the Na–Ru–O phase diagram.

Regardless of the additional complexities present in the O-rich regime, the isothermal phase diagram presented here establishes a reliable method for Ru-rich processing of NaRuO_2 , minimizing the substitution of nonmagnetic Na_{Ru} defects on the Ru triangular lattice. Compositions located in the three-phase NaRuO_2 – NaRu_2O_4 –Ru Alkemade triangle will reliably produce NaRuO_2 at the compositional invariant point where the ternary Alkemade triangle adjoins the vertex of the $\text{Na}_{3+x}\text{Ru}_{3-x}\text{O}_6$ single-phase region. Tuning the composition to produce NaRuO_2 at this vertex with minimal contributions from Ru-metal and NaRu_2O_4 enables stoichiometry control in a system with a complex phase diagram containing volatile elements.

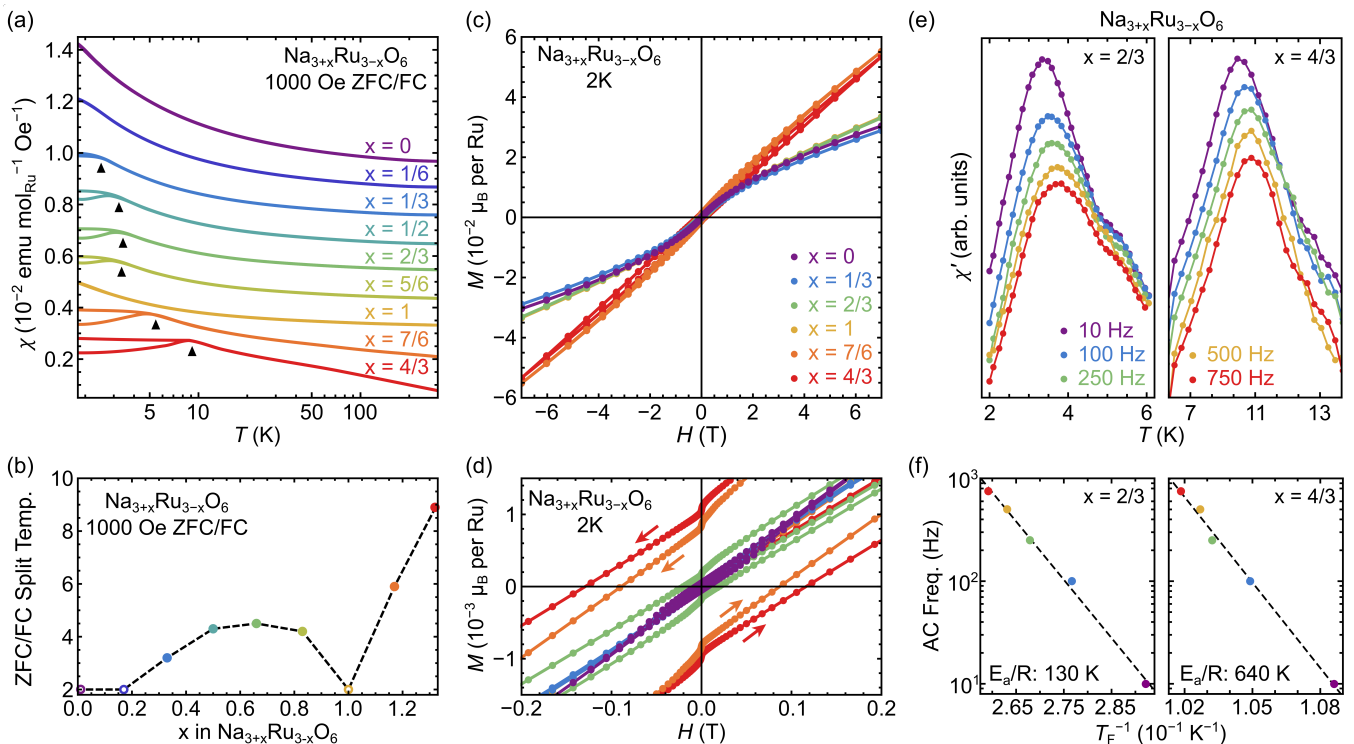


FIG. 5. (a) Temperature dependence of the ZFC and FC dc magnetic susceptibility for $\text{Na}_{3+x}\text{Ru}_{3-x}\text{O}_6$ alloys in an external applied field of 1000 Oe. Black triangles denote bifurcation temperatures of the ZFC/FC curves. (b) Compositional dependence of the ZFC/FC bifurcation temperature. Peaking for intermediate compositions, ZFC/FC splitting falls below 2 K for the nominal end members $x=0$ and 1. (c) Field dependence of the dc isothermal magnetization at 2 K with (d) magnified view about $H = 0$, highlighting non-zero coercivity for intermediate Na loading. Note that the coercivity vanishes to within the level of background for $x=0$ and 1. (e) Temperature dependence of the in-phase component χ' of the ac susceptibility in the absence of an external dc field for samples $x = 2/3, 4/3$ with (f) corresponding Arrhenius plot fit to empirical form $f \propto e^{-\frac{E_a}{RT_F}}$.

B. Magnetization and Electrical Transport

Our prior investigation on both the magnetic and electronic properties of stoichiometric NaRuO_2 identified the system as a magnetic insulator with a quantum disordered ground state [4]. Considering that Na_2RuO_3 was considered a distinct compound to date, the discovery of the $\text{Na}_{3+x}\text{Ru}_{3-x}\text{O}_6$ solid solution should provide an experimental route to exploring the physical properties and possibly unique crossovers (*e.g.* metal-to-insulator) between the endpoint members. However, literature reports on the magnetic and electronic properties of Na_2RuO_3 are varied. Much of the variation stems from the ambiguity whether the ordered or disordered polymorph is present. Even within studies focused predominantly on disordered Na_2RuO_3 or mixtures of the ordered/disordered phase, there are conflicting reports. Some works suggest insulating behavior with long-range antiferromagnetic order [21, 22], while others report a paramagnetic, moderately correlated electron metal with no observable magnetic excitations [23].

This lack of consensus on Na_2RuO_3 is likely driven by the existence of the $\text{Na}_{3+x}\text{Ru}_{3-x}\text{O}_6$ solid-solution. Since Na_2RuO_3 is not a line compound, the stoichiome-

try of a given synthesis is not well-defined. In the case of disordered Na_2RuO_3 , the majority of samples were produced as a product of decomposition reactions, yielding lattice parameters a : [3.11–3.17 Å] and c : [15.94–16.04 Å] [9, 23, 24]. One of the “hallmark” features of disordered Na_2RuO_3 in prior work is the merger of the (101) and (006) peak positions. In good agreement with prior literature, we find that the peak merger occurs with $a=3.11$ Å and $c=15.94$ Å. However, our nominal stoichiometry at that point is only $x=2/3$ instead of $x=1$. This is conceptually consistent with our findings that the Na–Ru–O systems require additional Na and O to compensate for volatility issues. Furthermore, Na incorporation continues well past the point of peak merger – and well beyond nominal Na_2RuO_3 (Fig. 3).

The $\text{Na}_{3+x}\text{Ru}_{3-x}\text{O}_6$ solid solution presents an opportunity to study the defect-sensitivity of NaRuO_2 and the consequence of diluting the Ru-sublattice. We first address the electrical resistivity to determine whether all members of the $\text{Na}_{3+x}\text{Ru}_{3-x}\text{O}_6$ solid solution remain insulating, or whether the Na_{Ru} defects cause any increase in the free carrier concentration. As illustrated in Fig. 4, the resistivity at room temperature for many of the series falls within the lightly doped semiconducting regime

(10-100 m Ω -cm), and rises exponentially with decreasing temperature. Both observations suggest that members of the $\text{Na}_{3+x}\text{Ru}_{3-x}\text{O}_6$ solid solution up to $x=2/3$ are insulators or small-gap semiconductors.

The isothermal resistivity at 300 K (Fig. 4(inset)) exhibits an exponential *increase* with Na content, contradicting the most facile defect formation (*e.g.* $\text{Na}_{\text{Ru}} + 2\text{h}$) and instead supports the localization of holes via a shift of Ru into a higher oxidation state. The influence of poorly screened, higher charged Ru^{4+} – coupled with increased alloy/disorder scattering likely contribute to the strong resistivity increases. Potentially more complex compensation reactions such as oxygen vacancies could be present, and more research (*e.g.* DFT defect studies) will be important for fully understanding the defect energetics in the alloys. We note here that members with higher Na content ($x \geq 1$) become progressively deliquescent and will condense atmospheric water on the surfaces, precluding reliable measurement of their resistivity.

The dc susceptibility data for select $\text{Na}_{3+x}\text{Ru}_{3-x}\text{O}_6$ compositions are plotted in Fig. 5(a). A manual vertical offset has been introduced to facilitate a visual qualitative comparison, and an unscaled set of magnetization curves is included in the supplementary information for comparison [25]. Notably, an onset of irreversibility in the ZFC/FC curves appears in compositions with noninteger x . This irreversibility is absent in the stoichiometric $x=0$ end member above 2 K. Then, as summarized in Fig. 5(b), ZFC/FC irreversibility onsets at finite x and increases in temperature as further disorder is introduced. Near the midpoint between NaRuO_2 and Na_2RuO_3 , the irreversibility temperature reaches a local maximum and then begins to decrease again as $x = 1$ is approached. In the nominal $x=1$ composition with uniform Ru^{4+} sites, the system naively assumes a $J_{\text{eff}} = 0$ nonmagnetic singlet state and irreversibility vanishes. With continued Na loading beyond $x = 1$, moments are reintroduced and a sharp reemergence of irreversibility occurs. It should be noted that as $x = 0, 1/6, 1$ samples exhibit no discernible splitting by 2 K (though the curvature of $x = 1/6$ is suggestive of a splitting proximal to 2K), this lower limit on the onset of an irreversibility temperature is denoted as open circles in Fig. 5(b).

As illustrated in Figs. 5(c,d), the main qualitative trends presented in Fig. 5(b) are also reflected in the compositional dependence of the dc magnetization. Compositions with higher irreversibility temperatures exhibit larger coercivity, particularly for those samples where $x > 1$ (Fig. 5(d)). Irreversibility in FC/ZFC data reflect that local Ru moments freeze, and Fig. 5(e) illustrates this freezing further in the Na-rich side of the phase diagram with ac-susceptibility measurements over the splitting temperature for $x=2/3$ and $x=4/3$. The ac-susceptibility data reveal a clear frequency-dependence associated with local moment freezing in both samples.

High activation energy barriers are obtained for both $x=2/3$ and $x=4/3$ (130 K and 640 K, respectively) when analysis is performed solely using the Arrhenius model.

Attempting to utilize alternative models (*e.g.*, Vogel-Fulcher) yield similarly unusual characteristic times. Understanding the freezing dynamics in the $\text{Na}_{3+x}\text{Ru}_{3-x}\text{O}_6$ alloys will require more detailed measurements and neutron scattering measurements on single crystals. However, qualitatively these results demonstrate that the chemical and valence disorder imparted by Na_{Ru} defects throughout the magnetic sublattice acts to initiate freezing, consistent with our prior work suggesting that NaRuO_2 possesses a quantum disordered ground state [4].

It is worth stressing here that even in the nominal $x = 0$ composition, a low-temperature cusp appears in the ac-susceptibility below 2 K [4]. Near 1.7 K, signs of partial moment freezing were observed, indicating a weak spin freezing transition and crossover in the low frequency spin dynamics. This crossover/partial freezing is likely driven by a small percentage of remnant Na defects ($\approx 1\%$). This is consistent with the amplification of the freezing onset upon the intentional introduction of additional Na defects along the solid solution line between NaRuO_2 and Na_2RuO_3 .

IV. CONCLUSIONS

Motivated by the need to control and understand defect relationships in the Heisenberg-Kitaev candidate material NaRuO_2 , we studied the chemical potential phase space surrounding NaRuO_2 . We discovered the existence of a full solid-solution $\text{Na}_{3+x}\text{Ru}_{3-x}\text{O}_6$ between NaRuO_2 ($x=0$) and disordered Na_2RuO_3 ($x=1$). While resistivity measurements demonstrate that all members of $\text{Na}_{3+x}\text{Ru}_{3-x}\text{O}_6$ are insulators, increased Na-incorporation into the alloy results in a glass-like freezing of local Ru moments between stoichiometric endpoints. At small x , this is conceptually consistent with moment dilution/induced freezing on a highly frustrated Ru^{3+} sublattice. Our study provides key information needed to control chemical disorder and off-stoichiometry in the Heisenberg-Kitaev candidate material NaRuO_2 .

V. ACKNOWLEDGMENTS

We acknowledge fruitful conversations with A. A. Aczel, G. Pokharel, and A. R. Ericks. This work was supported by the US Department of Energy (DOE), Office of Basic Energy Sciences, Division of Materials Sciences and Engineering under Grant No. DE-SC0017752. B.R.O. and P.M.S. both acknowledge financial support from the California NanoSystems Institute through the Elings Fellowship program. The research made use of the shared facilities of the NSF Materials Research Science and Engineering Center at UC Santa Barbara (DMR- 1720256). The UC Santa Barbara MRSEC is a member of the Materials Research Facilities Network. (www.mrfn.org). This work also

used facilities supported via the UC Santa Barbara NSF

Quantum Foundry funded via the Q-AMASE-i program under award DMR-1906325.

-
- [1] L. Balents, Spin liquids in frustrated magnets, *Nature* **464**, 199 (2010).
- [2] Y. Zhou, K. Kanoda, and T.-K. Ng, Quantum spin liquid states, *Rev. Mod. Phys.* **89**, 025003 (2017).
- [3] C. Broholm, R. J. Cava, S. A. Kivelson, D. G. Nocera, M. R. Norman, and T. Senthil, Quantum spin liquids, *Science* **367**, eaay0668 (2020).
- [4] B. R. Ortiz, P. M. Sarte, A. H. Avidor, A. Hay, E. Kenney, A. I. Kolisneikov, A. A. Aczel, C. Brown, C. Wang, M. J. Graf, R. Seshadri, L. Balents, and S. D. Wilson, Quantum Disordered Ground State in the Heisenberg-Kitaev Candidate NaRuO₂, Preprint available at Research Square <https://doi.org/10.21203/rs.3.rs-1551865/v1>.
- [5] J. A. M. Paddison, M. Daum, Z. Dun, G. Ehlers, Y. Liu, M. B. Stone, H. Zhou, and M. Mourigal, Continuous excitations of the triangular-lattice quantum spin liquid YbMgGaO₄, *Nat. Phys.* **13**, 117 (2017).
- [6] Y. Li, YbMgGaO₄: A Triangular-Lattice Quantum Spin Liquid Candidate, *Adv. Quantum Technol.* **2**, 1900089 (2019).
- [7] R. Dally, R. J. Clément, R. Chisnell, S. Taylor, M. Butala, V. Doan-Nguyen, M. Balasubramanian, J. W. Lynn, C. P. Grey, and S. D. Wilson, *J. Cryst. Growth* **459**, 203 (2017).
- [8] S. J. Clarke, A. J. Fowkes, A. Harrison, R. M. Ibberson, and M. J. Rosseinsky, Synthesis, structure, and magnetic properties of NaTiO₂, *Chem. Mater.* **10**, 372 (1998).
- [9] K. M. Mogare, K. Friese, W. Klein, and M. Jansen, Syntheses and crystal structures of two sodium ruthenates: Na₂RuO₄ and Na₂RuO₃, *Z. fur Anorg. Allg. Chem.* **630**, 547 (2004).
- [10] A. A. Coelho, *TOPAS* and *TOPAS-Academic*: an optimization program integrating computer algebra and crystallographic objects written in C++, *J. Appl. Crystallogr.* **51**, 210 (2018).
- [11] K. Momma and F. Izumi, *VESTA3* for three-dimensional visualization of crystal, volumetric and morphology data, *J. Appl. Crystallogr.* **44**, 1272 (2011).
- [12] M. Shikano, C. Delmas, and J. Darriet, NaRuO₂ and Na_xRuO₂ · yH₂O: New Oxide and Oxyhydrate with Two Dimensional RuO₂ Layers, *Inorg. Chem.* **43**, 1214 (2004).
- [13] M. Shikano, R. K. Kremer, M. Ahrens, H.-J. Koo, M.-H. Whangbo, and J. Darriet, Synthesis and characterization of a magnetic semiconductor Na₂RuO₄ containing one-dimensional chains of Ru⁶⁺, *Inorg. Chem.* **43**, 5 (2004).
- [14] K. A. Regan, Q. Huang, and R. J. Cava, Isolated spin 3/2 plaquettes in Na₃RuO₄, *J. Solid State Chem.* **178**, 2104 (2005).
- [15] J. Allred, L. Wang, P. Khalifah, and R. J. Cava, Na₂₇Ru₁₄O₄₈: A new mixed-valence sodium ruthenate with magnetic heptameric plaquettes, *J. Solid State Chem.* **184**, 44 (2011).
- [16] K. A. Regan, Q. Huang, M. Lee, A. P. Ramirez, and R. J. Cava, Structure and magnetism of NaRu₂O₄ and Na_{2.7}Ru₄O₉, *J. Solid State Chem.* **179**, 195 (2006).
- [17] B. R. Ortiz, K. Gordiz, L. C. Gomes, T. Braden, J. M. Adamczyk, J. Qu, E. Ertekin, and E. S. Toberer, Carrier density control in Cu₂HgGeTe₄ and discovery of Hg₂GeTe₄ via phase boundary mapping, *J. Mater. Chem. A* **7**, 621 (2019).
- [18] S. Ohno, U. Aydemir, M. Amsler, J.-H. Pöhls, S. Chanakian, A. Zevalkink, M. A. White, S. K. Bux, C. Wolverton, and G. J. Snyder, Achieving $zT \geq 1$ in inexpensive Zintl phase Ca₉Zn_{4+x}Sb₉ by phase boundary mapping, *Adv. Funct. Mater.* **27**, 1606361 (2017).
- [19] S. Ohno, K. Imasato, S. Anand, H. Tamaki, S. D. Kang, P. Gorai, H. K. Sato, E. S. Toberer, T. Kanno, and G. J. Snyder, Phase boundary mapping to obtain *n*-type Mg₃Sb₂-based thermoelectrics, *Joule* **2**, 141 (2018).
- [20] C. M. Crawford, B. R. Ortiz, P. Gorai, V. Stevanovic, and E. S. Toberer, Experimental and computational phase boundary mapping of Co₄Sn₆Te₆, *J. Mater. Chem. A* **6**, 24175 (2018).
- [21] J. C. Wang, J. Terzic, T. F. Qi, F. Ye, S. J. Yuan, S. Aswartham, S. V. Streltsov, D. I. Khomskii, R. K. Kaul, and G. Cao, Lattice-tuned magnetism of Ru⁴⁺ (*4d⁴*) ions in single crystals of the layered honeycomb ruthenates Li₂RuO₃ and Na₂RuO₃, *Phys. Rev. B* **90**, 161110 (2014).
- [22] V. V. Gapontsev, E. Z. Kurmaev, C. I. Sathish, S. Yun, J.-G. Park, and S. V. Streltsov, Spectral and magnetic properties of Na₂RuO₃, *J. Phys.: Condens. Matter* **29**, 405804 (2017).
- [23] L. S. I. Veiga, M. Etter, E. Cappelli, H. Jacobsen, J. G. Vale, C. D. Dashwood, D. Le, F. Baumberger, D. F. McMorrow, and R. S. Perry, Correlated electron metal properties of the honeycomb ruthenate Na₂RuO₃, *Phys. Rev. Materials* **4**, 094202 (2020).
- [24] M. Tamaru, X. Wang, M. Okubo, and A. Yamada, Layered Na₂RuO₃ as a cathode material for Na-ion batteries, *Electrochem. commun.* **33**, 23 (2013).
- [25] See Supplemental Information for further details.